JBC RESEARCH ARTICLE

Pre-rRNA facilitates the recruitment of RAD51AP1 to DNA double-strand breaks

Received for publication, January 4, 2024, and in revised form, February 2, 2024 Published, Papers in Press, February 24, 2024,
https://doi.org/10.1016/j.jbc.2024.107115

Linlin Chen[1,2], **Xiaochen Gai**[2,3,4], **and Xiaochun Yu**[2,3,4,*]

From the [1]*School of Life Sciences, Fudan University, Shanghai, China;* [2]*School of Life Sciences, Westlake University, Hangzhou, Zhejiang, China;* [3]*Westlake Laboratory of Life Sciences and Biomedicine, Hangzhou, Zhejiang, China;* [4]*Institute of Basic Medical Sciences, Westlake Institute for Advanced Study, Hangzhou, Zhejiang Province, China*

Reviewed by members of the JBC Editorial Board. Edited by Patrick Sung

RAD51-associated protein 1 (RAD51AP1) is known to promote homologous recombination (HR) repair. However, the precise mechanism of RAD51AP1 in HR repair is unclear. Here, we identify that RAD51AP1 associates with pre-rRNA. Both the N terminus and C terminus of RAD51AP1 recognize pre-rRNA. Pre-rRNA not only colocalizes with RAD51AP1 at double-strand breaks (DSBs) but also facilitates the recruitment of RAD51AP1 to DSBs. Consistently, transient inhibition of pre-rRNA synthesis by RNA polymerase I inhibitor suppresses the recruitment of RAD51AP1 as well as HR repair. Moreover, RAD51AP1 forms liquid–liquid phase separation in the presence of pre-rRNA *in vitro*, which may be the molecular mechanism of RAD51AP1 foci formation. Taken together, our results demonstrate that pre-rRNA mediates the relocation of RAD51AP1 to DSBs for HR repair.

Homologous recombination (HR) is a highly precise and reliable approach for the repair of DNA double-strand breaks (DSBs), and this cellular process relies on the availability of homologous sequences in genomic DNA. This high fidelity and complicated repair pathway maintains genomic integrity (1–4) and comprises several major steps. In the presynaptic stage, the single-strand overhang at DSB ends is stabilized by the replication protein A (RPA) complex. Subsequently, RAD51 replaces the RPA complex and recognizes the single-strand overhang forming a nucleoprotein filament. This interaction promotes homologous strand invasion and exchange during the synaptic stage (5). DNA is replicated using homologous strands as the templates, and the intermediate DNA structures named Holliday junctions are resolved for the completion of the repair (6, 7).

Many layers of regulation in HR repair have been revealed over the past few decades (8–10). In particular, RAD51 associates with several key factors that modulate RAD51–ssDNA filaments, and one of these key factors is RAD51-associated protein 1 (RAD51AP1). Using yeast two-hybrid approach, RAD51AP1 was identified as a RAD51-binding partner (11). The interaction region has been mapped at the C terminus of RAD51AP1 (12). It has been shown that RAD51AP1 binds DNA, particularly the D-loop, a DNA intermediate during RAD51 filament invasion into homologous strand (13–16). Thus, it regulates the recombinase activities of RAD51 during HR. When RAD51AP1 is depleted in cells, it results in increased sensitivity of the cells to mitomycin C[6], leading to heightened susceptibility to DNA damage and an increased incidence of chromatid breaks.

Interestingly, in addition to the DNA binding, RAD51AP1 also recognizes RNA. It tethers RNA for the R-loop formation, which is prerequisite step for the RAD51-dependnet D-loop during HR repair (17). In addition, earlier studies also show that RAD51AP1 associates with TERRA long noncoding RNA for telomere maintenance and extension, particularly in the context of alternative lengthening of telomeres (18, 19). Collectively, these lines of evidence suggest that the RNA-binding activity of RAD51AP1 may play an important role to maintain genomic stability.

To identify other RNA species that are associated with RAP51AP1, we performed photoactivatable ribonucleoside-enhanced crosslinking and immunoprecipitation (PAR-CLIP) assays and searched for RAP51AP1-binding RNA. Surprisingly, we identified pre-rRNA as an important functional partner of RAP51AP1 during HR repair. This study may reveal the molecular mechanism by which pre-rRNA mediates the relocation of RAD51AP1 to DSBs.

Results

RAD51AP1 interacts with pre-rRNA

To unbiasedly reveal the major RNA species that are recognized by RAD51AP1, we established 293T cells stably expressing RAD51AP1 and used this cell line to perform PAR-CLIP assays. Surprisingly, we found that the major RNA species that associates with RAD51AP1 is rRNA (Fig. 1*A*). The sequencing reads cover the whole region of 45S pre-rRNA, including 5′ external transcribed spacer, 18S, internal transcribed spacer 1 (ITS1), 5.8S, ITS2, 28S, and 3′ external transcribed space regions (Fig. S1*A*). Moreover, the rRNA-associated with RAD51AP1 prior to RNA-Seq was remarkably enriched compared with the mock samples, suggesting that rRNA identified in the PAR-CLIP assays is not a common

* For correspondence: Xiaochun Yu, yuxiaochun@westlake.edu.cn.

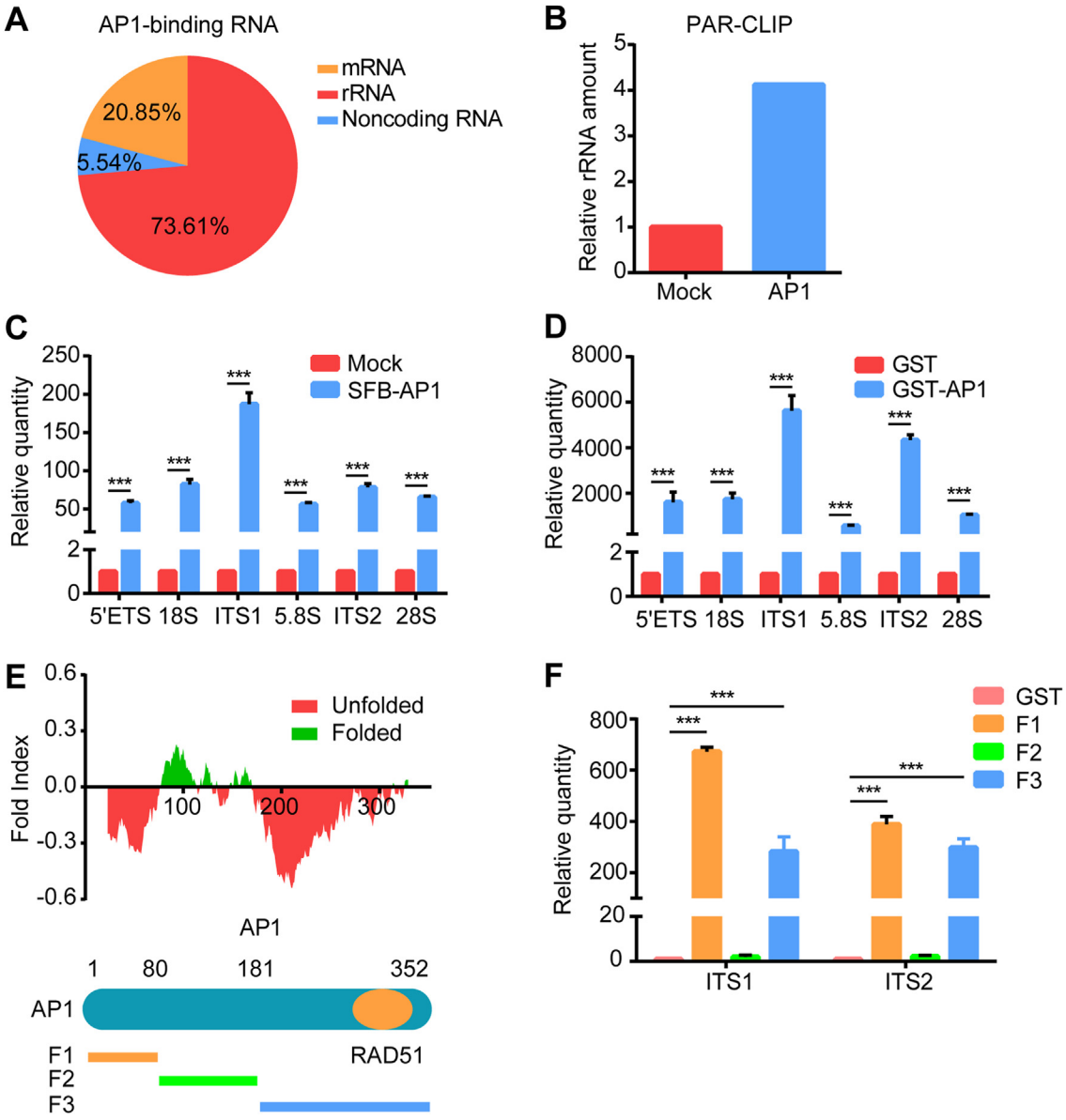

Figure 1. RAD51AP1 is associated with pre-rRNA. *A* and *B*, TopBP1 specifically recognizes pre-rRNA. *A*, the proportion of RAD51AP1-associated RNA based on PAR-CLIP. *B*, total sequencing amount on 45S recombinant DNA loci from SFB-vector or SFB-RAD51AP1 purification. *C*, validation of the interaction between RAD51AP1 and pre-rRNA. Following PAR-CLIP, qPCR was performed to examine RAD51AP1-interacted pre-rRNAs. *D*, recombinant RAD51AP1 binds pre-rRNA *in vitro*. GST or GST-RAD51AP1 proteins were incubated with total RNAs extracted from 293T cells. qPCR was performed to examine GST-RAD51AP1-associated pre-rRNAs. *E*, schematics of RAD51AP1-disordered regions (*upper*) and truncation mutants (*lower*). *F*, the disorder regions of RAD51AP1 bind to pre-rRNA. Recombinant RAD51AP1-truncated proteins were incubated with total RNAs. Pull down-qPCR was used to determine the interaction between proteins and pre-rRNAs. Data are shown as mean ± SD. ***$p < 0.001$. GST, glutathione-S-transferase; PAR-CLIP, photoactivatable ribonucleoside-enhanced crosslinking and immunoprecipitation; qPCR, quantitative PCR; RAD51AP1, RAD51-associated protein 1.

RNA contamination but specifically associated with RAD51AP1 (Fig. 1*B*). To further validate this interaction, we performed RNA-binding protein immunoprecipitation and quantitative PCR (qPCR) assays as well as glutathione-*S*-transferase (GST)-RAD51AP1 fusion protein pull down and qPCR assays (pull down–qPCR) (Fig. 1, *C* and *D*) and found that RAD51AP1 is associated with rRNA, particularly the ITS1 and ITS2 regions. Collectively, these results demonstrate that pre-rRNA is a binding partner of RAD51AP1.

To identify the interaction region(s) on RAD51AP1, we generated the recombinant truncation mutants of RAD51AP1 based on the predicted folding and disorder regions (Fig. 1*E*) and performed pull down–qPCR. We found that the N-terminal and C-terminal disorder regions but not the folded region in the middle (Fig. 1*F*) recognized pre-rRNA. Moreover, we also examined if RAD51AP1 nonspecifically recognizes RNA. We randomly explored 7SK and MALATA, two highly expressed long noncoding RNA. However, RAD51AP1 did not associate with these RNA species (Fig. S1*B*). Of note, RAD51AP1 but not RAD51 bound with pre-rRNA, further suggesting the specific interaction between RAD51AP1 and pre-rRNA (Fig. S1*C*).

Taken together, these results indicate that RAD51AP1 selectively interacts with pre-rRNA.

Pre-rRNA and RAD51AP1 are accumulated at DSBs

Earlier studies have shown that pre-rRNA mediates DSB response (20). Thus, it is possible that pre-rRNA is a functional partner of RAD51AP1 during DSB repair. To investigate the cellular localizations of pre-rRNA and RAD51AP1 in response to DSBs, we treated cells with ionizing radiation (IR). Interestingly, we observed a gradually increased protein level of RAD51AP1 in the chromatin fraction following IR treatment (Fig. S2). The nuclear foci of RAD51AP1 were clearly observed 8 h following IR treatment and were largely colocalized with γH2AX, the surrogate marker of DSBs (Fig. 2*A*). Interestingly, with RNA FISH assays, we found that pre-rRNA colocalized with RAD51AP1 at the nuclear foci (Fig. 2, *B* and *C*).

To further examine the colocalization of pre-rRNA and RAD51AP1, we performed chromatin immunoprecipitation (ChIP) assay in HCT116 cell harboring an I-SceI restriction enzyme cutting site. When I-SceI was expressed in the cells, it generated a sole DSB (21). Using chromatin immunoprecipitation assays (ChIP), we found that γH2AX was remarkably enriched at the I-SceI-induced DSB. Consistently, both rRNA and RAD51AP1 were enriched at the DSB (Fig. 2*D*). Taken

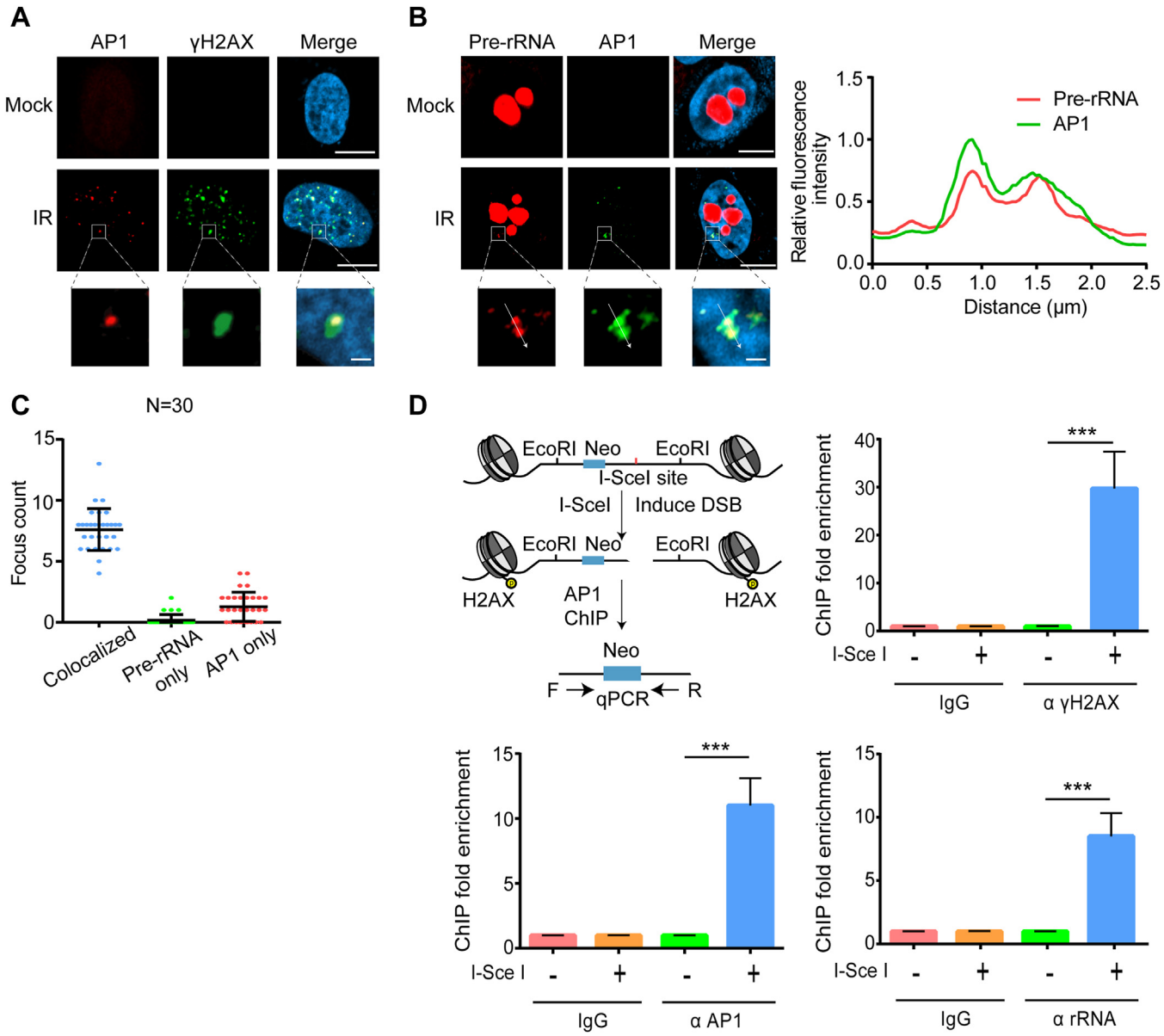

Figure 2. Pre-rRNA colocalizes with RAD51AP1 at DSBs. *A*, RAD51AP1 is localized at irradiation-induced foci (IRIF). U2OS cells were treated with 20 Gy irradiation and were stained with anti-RAD51AP1 and anti-γH2AX antibodies. *B*, pre-rRNA is colocalized with RAD51AP1 at IRIF. Following 20 Gy irradiation, RNA FISH and immunostaining were performed to detect pre-rRNA and RAD51AP1 foci (*left*). The colocalization of pre-rRNA and RAD51AP1 was analyzed (*right*). *C*, quantitative analysis of pre-rRNA and RAD51AP1 foci. *D*, pre-rRNA localizes at I-SceI-induced DSB. I-SceI was induced to create a solo DSB. The accumulation of pre-rRNAs, RAD51AP1, or γH2AX at the DSB was determined by ChIP–qPCR. IgG served as a negative control. Data are shown as mean ± SD. ***$p < 0.001$. Scale bar represents 10 μm. Zoom in scale bar represents 1 μm. ChIP, chromatin immunoprecipitation; DSB, double-strand break; IgG, immunoglobulin G; qPCR, quantitative PCR; RAD51AP1, RAD51-associated protein 1.

together, these results suggest that both pre-rRNA and RAD51AP1 are recruited to DSBs.

Pre-rRNA regulates the relocation of RAD51AP1 to DSBs

To examine the functional interactions between pre-rRNA and RAD51AP1, we used siRNA to knock down the level of RAD51AP1 (Fig. S3*A*), thus abolished the foci of RAD51AP1 (Fig. S3*B*). However, loss of RAD51AP1 did not affect the foci of pre-rRNA (Fig. S3*C*), suggesting that RAD51AP1 does not mediate the relocation of pre-rRNA to DSBs.

Pre-rRNA is transcribed from recombinant DNA loci by RNA polymerase I (pol I) (22). To examine whether pre-rRNA regulates the relocation of RAD51AP1 to DSBs, we transiently treated cells with the pol I inhibitor BMH-21 for 2 h to abrogate pre-rRNA biogenesis (23). Interestingly, the transient pol I inhibitor treatment but not pol II or pol III inhibitor treatment drastically reduced the foci of RAD51AP1 (Fig. 3*A*). Of note, because of long half-lives of mature rRNA, the transient pol I inhibitor treatment did affect neither the levels of mature rRNA nor the global protein biogenesis (Fig. 3*B*). Moreover, we treated cells with RNase A to remove RNA species at DSBs (24). Again, the foci of RAD51AP1 were abolished (Fig. 3*C*). Next, when we deleted either RNA-binding regions of RAD51AP1, the mutants could not relocate to DSBs (Fig. 3*D*). Collectively, these results demonstrate that pre-rRNA mediates the nuclear foci of RAD51AP1 in response to DSBs. In addition, we transiently treated HCT116 with I-SceI site with pol I inhibitor. Again, compared with pol II or pol III inhibitor treatment, pol I inhibitor treatment abolished the enrichment of RAD51AP1 (Fig. 3*E*), suggesting that pre-rRNA facilitates the recruitment of RAD51AP1 to DSBs.

Since RAD51AP1 plays an important role for HR repair, we measured HR efficacy using a well-established GFP reporter assay (20)(Fig. 4*A*). Notably, with either knock down of RAD51AP1 or pol I inhibitor treatment, GFP positive populations were reduced (Fig. 4, *B* and *C*), suggesting that pre-rRNA and RAD51AP1 mediate HR repair.

Pre-rRNA facilitates RAD51AP1 liquid–liquid phase separation

In response to DSBs, pre-rRNA-mediated foci formation of RAD51AP1 represents a unique biomolecular condensate (25). Since RNA often acts as a scaffold for liquid–liquid phase separation (LLPS) (26), we investigate whether pre-rRNA mediates LLPS of RAD51AP1 using *in vitro* LLPS assays. We incubated pre-rRNA isolated from 293T cells with recombinant GFP-RAD51AP1 protein *in vitro*. We found that RAD51AP1 exhibited pre-rRNA concentration-dependent LLPS (Fig. 5*A*). The N terminus (F1) or C terminus (F3) of RAD51AP1 was also able to form LLPS in the presence of pre-rRNA (Fig. 5*B*). In sharp contrast, RNase A treatment abolished pre-rRNA-dependent LLPS of RAD51AP1 (Fig. 5*C*). Moreover, we assessed the mobility of RAD51AP protein in the presence of pre-rRNA and found that RAD51AP1 exhibited a notable capacity for condensate fusion (Fig. 5*D*). Fluorescent recovery after photobleaching (FRAP) analysis showed the high mobility rate of RAD51AP1 (Fig. 5*E*). Collectively, these results demonstrate that pre-rRNA facilitates the LLPS of RAD51AP1 *in vitro*, which could be the molecular basis of DSB-induced foci of RAD51AP1.

Discussion

In this study, we show that pre-rRNA associates with RAD51AP1 at DSBs, which plays a key role for HR repair (Fig. 6). Since rRNA accounts for 80∼90% of the total RNA in cells (27), it is often considered as RNA contamination. Thus, before RNA-Seq analysis, it is always precleared from the testing samples. Surprisingly, we found that pre-rRNA is a functional partner of RAD51AP1 during HR repair. RAD51AP1 selectively recognizes pre-rRNA *via* the N-terminal and C-terminal disordered regions. Usually, the interactions between proteins and RNAs are multivalent interactions involving multiple binding sites on proteins for higher affinities to form stable ribonucleoproteins (28). Here, the pre-rRNA binding sites are coincided with the DNA-binding sites of RAD51AP1. It is likely that RAD51AP1 uses the same nucleic acid–binding motifs to recognize both RNA and DNA. It is possible that sequential binding to RNA and DNA allows RAD51AP1 to fulfill its functions in HR repair. In particular, RAD51AP1 may first recognize pre-rRNA for the relocation to DSBs and then change the binding partners to other RNA species or DNA for the next step of HR. However, the detailed process should be elucidated in the future.

Pre-rRNA is a mixture of several intermediates during the rRNA processing. Here, we detected the whole regions of 45S during the interaction analysis. From the PAR-CLIP assays, the RNA sequence reads are mainly on the 28S and 18S regions. Consistently, 28S and 18S are two predominant pre-rRNA species in nucleus. Moreover, both 28S and 18S are well folded and resistant to environmental RNase. Thus, it is very easy to detect 28S and 18S. However, from other interaction assays, the ITS1 and ITS2 regions are also remarkably associated with RAD51AP1. It is possible that RAD51AP1 associates with multiple forms of pre-rRNA during HR repair.

Here, we have shown that pre-rRNA mediates the relocation of RAD51AP1 to DSBs. Our earlier studies have shown that pre-rRNA was recruited by MDC1 to DSBs (20). Once pre-rRNA was recruited, it is recognized by DSB repair factors, such as RAD51AP1. The *in vitro* LLPS analyses indicate that pre-rRNA may serve as the scaffold to mediate the foci formation of RAD51AP1 at DSBs. Since DSB-induced foci formation of RAD51AP1 is a unique type of LLPS, these *in vitro* LLPS analyses may provide molecular basis by which pre-rRNA mediates the foci formation of RAD51AP1 in cells. Once RAD51AP1 reaches DSBs, it may interact with other functional partners for the R-loop and D-loop formation and

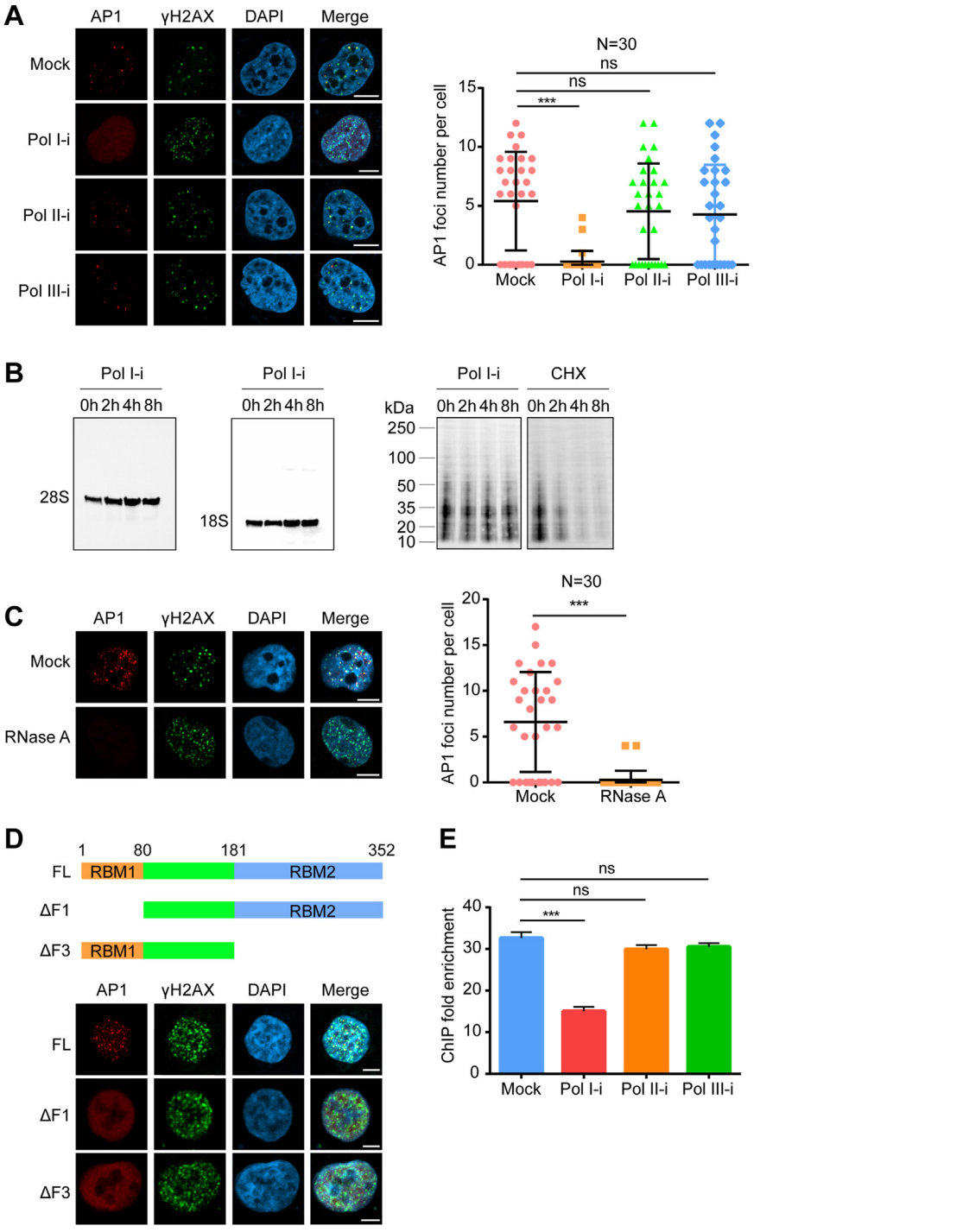

Figure 3. Pre-rRNA mediates RAD51AP1 foci formation. *A*, RNA polymerase I (pol I) inhibitor treatment suppresses RAD51AP1 foci formation. Two hours after vehicle, pol I, pol II, or pol III inhibitor treatment, HeLa cells were exposed to 20 Gy of irradiation. Foci formation of RAD51AP1 and γH2AX was examined by immunofluorescence (IF) staining (*left*). Foci number per cell was analyzed (*right*). *B*, transient RNA pol I inhibitor treatment does not affect mature rRNA production and protein synthesis. Mature 28S and 18S rRNAs were examined by Northern blot. Neosynthesized protein was determined by Western blot. Cycloheximide-treated cells served as positive control. *C*, RAD51AP1 foci formation is mediated by RNA. After 20 Gy irradiation, HeLa cells were treated with RNase A before fixation. RAD51AP1 foci were detected by IF staining (*left*). Foci number per cell is quantified (*right*). *D*, RNA-binding regions are important for the recruitment of RAD51AP1 to DSBs. Full length (FL) or RNA-binding region–deleted mutants (ΔF1 and ΔF3) of RAD51AP1 were expressed in HCT116 cells. After 20 Gy irradiation, IRIF was examined by immunostaining. *E*, RNA pol I inhibitor treatment suppresses the accumulation of RAD51AP1 at DSBs. Following pol I, pol II, or pol III inhibitor treatment, the enrichment of RAD51AP1 at I-SceI-induced solo DSB sites was examined by ChIP–qPCR. Data are shown as mean ± SD. ***$p < 0.001$. Scale bars represent 10 μm. ChIP, chromatin immunoprecipitation; qPCR, quantitative PCR; RAD51AP1, RAD51-associated protein 1; RBM, RNA-binding motif.

facilitates RAD51 filament invasion into the homologous strand (13, 17, 29). Thus, both pre-rRNA and RAD51AP1 govern HR repair.

In addition, although we have identified that pre-rRNA is recognized by RAD51AP1. It is possible that other DSB repair factors may also recognize pre-rRNA for DSB repair.

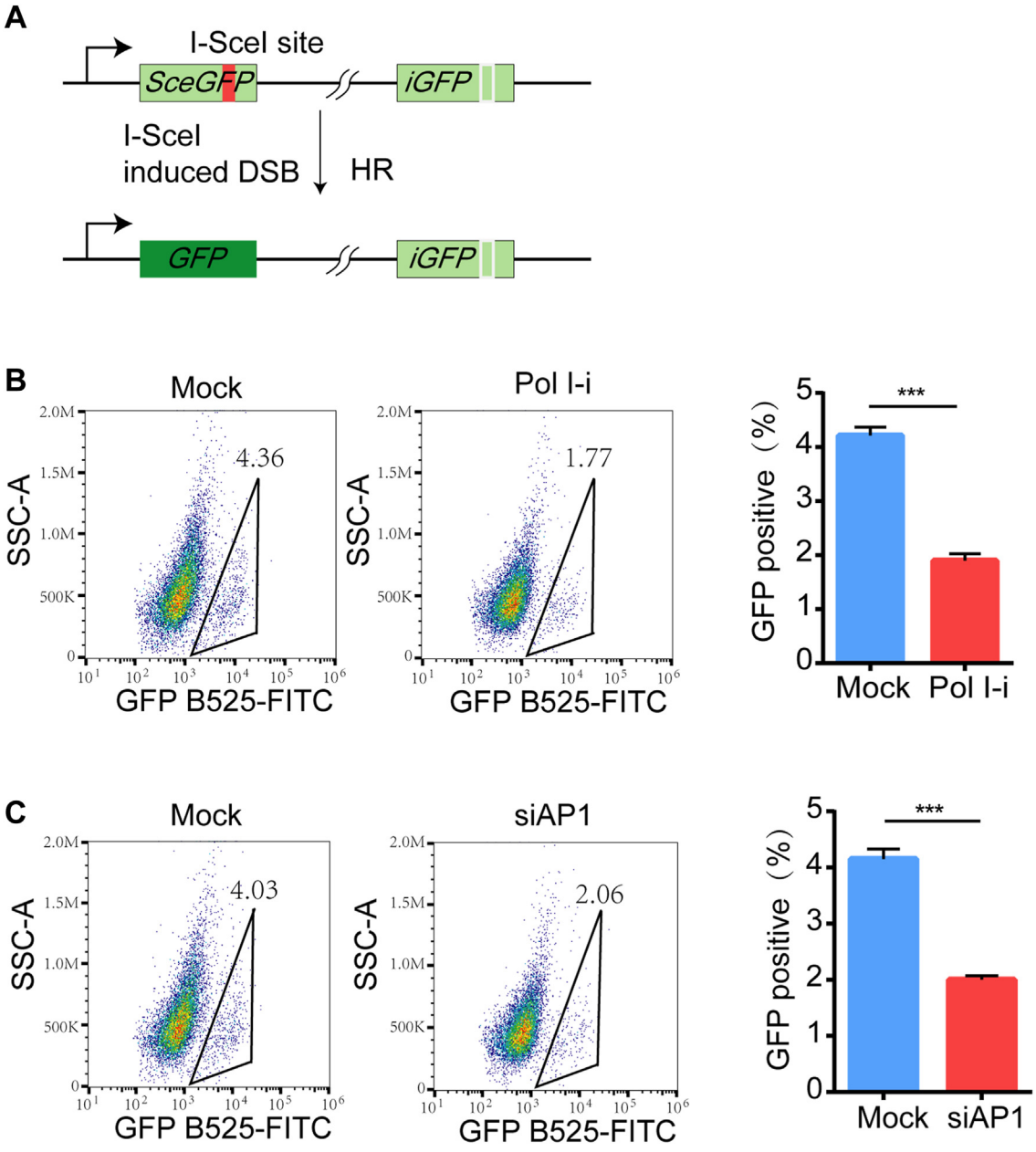

Figure 4. Pre-rRNA regulates HR efficiency. *A*, schematic of DR-GFP reporter system utilized to determine HR efficiency. *B*, RNA polymerase I inhibition suppresses HR repair. Flow cytometry was performed to evaluate the effect of BMH-21 treatment on HR efficiency (*left*). The GFP-positive population representing HR-repaired cells was analyzed (*right*). *C*, RAD51AP1 depletion impairs HR repair efficiency. DR-GFP-U2OS cells were transfected with control or RAD51AP1-trageted siRNAs. HR efficiency was assessed by quantifying GFP-positive cells. Data are shown as mean ± SD. ***$p < 0.001$. HR, homologous recombination.

However, we did not find that RAD51 can interact with pre-rRNA (Fig. S1*C*), excluding pre-rRNA as a direct partner of RAD51.

Experimental procedures

Plasmids

Human full-length RAD51AP1 (National Center for Biotechnology Information Gene ID: 10635) was synthesized by Tsingke Biotechnology company. RAD51AP1 complementary DNA (cDNA) was cloned into SFB vector for its expression in mammalian cells. Full-length or fragments of RAD51AP1(F1, amino acids 1–80; F2, amino acids 81–180; and F3, amino acids 181–352) were cloned into pGEX-4T1 vector for recombinant protein purification. Enhanced GFP (EGFP) was added to the N terminus of RAD51AP1 to purify EGFP-tagged proteins.

Antibodies

Antibodies were purchased from respective companies: anti-FLAG (Sigma; rabbit, catalog no.: F7425; mouse, catalog no.: F1804), anti-γH2AX (Novus; rabbit, catalog no.: NB100-384; homemade, mouse), anti-RAD51AP1 (Proteintech; rabbit, catalog no.: 11255-1-AP), anti-rRNA (Novus; rabbit, catalog no.: NB100-662), IgG (CST; rabbit, catalog no.: 2729),

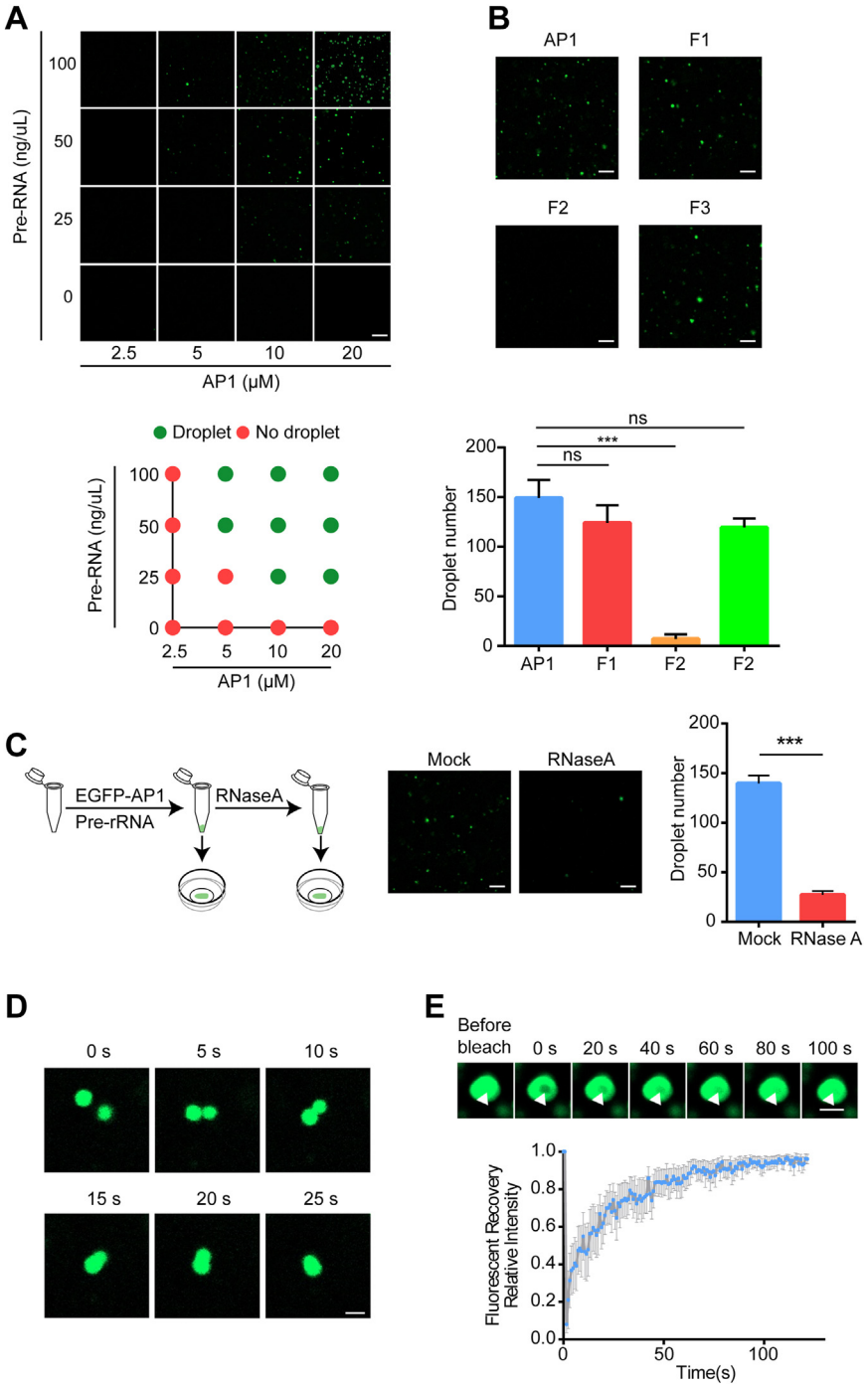

Figure 5. Pre-rRNA promotes RAD51AP1 liquid–liquid phase separation (LLPS). *A*, pre-rRNA facilitates LLPS of RAD51AP1. Increasing concentrations of recombinant RAD51AP1 were incubated with growing concentrations of pre-rRNA in 10% PEG8000 buffer for 10 min. LLPS was examined by microscopy (*upper*). Corresponding square networks represented droplet formation in different concentrations (*lower*). Scale bar represents 10 μm. *B*, the RNA-binding regions of RAD51AP1 form LLPS with pre-RNA. Full-length or deleted mutants of RAD51AP1 was incubated with 50 ng/μl pre-rRNA in 10% PEG8000 buffer for 10 min. Scale bar represents 10 μm. *C*, RNA depletion impairs RAD51AP1 LLPS. Schematic of RNase A treatment in examining RAD51AP1 LLPS (*left*). The droplets of RAD51AP1 were determined by microscopy (*right*). Scale bar represents 10 μm. *D*, microscopy images of individual RAD51AP1 droplet collisions at indicated time points. Scale bar represents 1 μm. *E*, representative micrographs of RAD51AP1 droplets before and after photobleaching (*upper*). FRAP quantification of droplets over a period of 120 s (*lower*). Scale bar represents 1 μm. Data are shown as mean ± SD, ***$p < 0.001$. FRAP, fluorescent recovery after photobleaching; RAD51AP1, RAD51-associated protein 1.

antipuromycin (Sigma–Aldrich; mouse, catalog no.: 12D10), anti-GAPDH (CST; rabbit, catalog no.: 5174), anti-H3 (CST; rabbit, catalog no.: 4499S), anti-RAD51 (Abcam; rabbit, catalog no.: ab133534), and anti-RPA (Novus; rabbit, catalog no.: NBP1-23017).

RNA interference

Cells were transfected with siRNAs against nonspecific control or RAD51AP1(5 nM) by Lipofectamine RNAiMax (Invitrogen) according to the manufacturer's instructions. The sequences of the siRNAs are shown in Table S1.

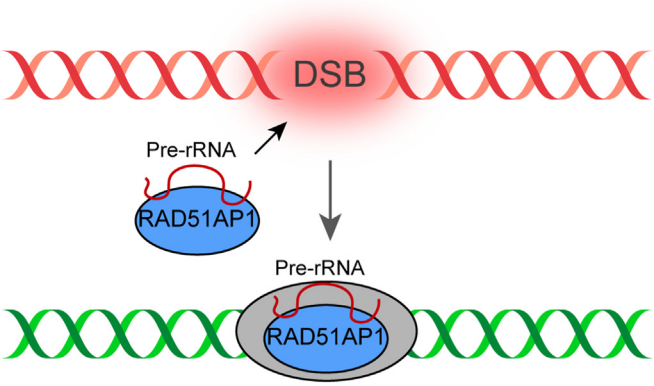

Figure 6. The schematic model of pre-rRNA-mediating RAD51AP1 foci formation in HR repair. HR, homologous recombination; RAD51AP1, RAD51-associated protein 1.

Cell culture and transfection

HeLa, 293T, HCT116, and U2OS cells were purchased from American Type Culture Collection. Cells were cultured at 37 °C with 5% CO_2 in Dulbecco's modified Eagle's medium (Gibco) supplemented with 10% fetal bovine serum (Cellmax) and 1% penicillin/streptomycin (Sangon Biotech). Plasmid transfection was performed using Lipofectamine 2000 according to the manufacturer's instruction.

Purification of recombinant proteins

GST-tagged RAD51AP1 proteins were expressed in *Escherichia coli* BL21 cells and purified using glutathione Sepharose (GE) and SuperDex 200 (Cytiva) with FPLC (Union Bio).

PAR-CLIP

293T cells stably expressing SFB-tagged RAD51AP1 were cultured 14 h in Dulbecco's modified Eagle's medium supplemented with 6-SG (100 μM). These cells were washed with cold PBS buffer twice and were then crosslinked with 0.4 J/cm^2 total energy of 365 nm UV light. NETN300 buffer (50 mM Tris–HCl [pH 8.0], 300 mM NaCl, 0.5 mM EDTA, and 0.5% IGEPAL CA-630) containing protease inhibitor cocktail, and RNase inhibitor was used to harvest and lyse cells. The cell lyses was incubated with High Capacity Streptavidin Resin (Thermo Fisher) for 2 h at 4 °C. After three times of washes with NETN300 buffer, the beads were treated with 2 mg/ml biotin at 4 °C to elute proteins off. The eluent was incubated with FLAG-M2 beads for 2 h at 4 °C. The beads were then washed by NETN300 buffer for three times. Protein-associated RNAs were released by proteinase K and extracted by phenol/chloroform. Purified RNAs were used for RNA-Seq or qPCR.

RNA-Seq was performed by LC-Bio Technology CO, Ltd. The trimmed RNA-Seq reads were aligned to the human genome assembly CHM13 v2.0 using STAR version 2.7.6a. Gene count data were generated using feature Counts, version 2.0.2. The unaligned reads were converted to FASTA format, and the reads shorter than 18 nt were excluded using SeqKit, version 2.1.0.

GST-protein pull down assay

For GST fusion protein pull down assay, proteins (5 μg), RNAs (5 μg), and Glutathione Sepharose 4B (200 μl) beads were incubated in 500 μl NETN100 buffer at 4 °C for 2 h. Then, the Glutathione Sepharose 4B beads were centrifuged and washed with NETN300 buffer. Protein-associated RNA was extracted by Trizol (Invitrogen). The RNAs were used to synthesize cDNA with Hifair III first Strand cDNA Synthesis SuperMix kit (Yeasen). SYBR Green–based qPCR was performed on CFX connect Real-Time PCR Detection System (Bio-Rad). The primers are listed in Table S1.

I-SceI-induced DSB system

HCT116 cells harboring a solo I-SceI site on the X chromosome were infected with pCW-HA-I-SceI-GR plasmids. I-SceI expression was induced by doxycycline. Acetonide was applied to facilitate the translocation of I-SceI into the nucleus. Finally, the I-SceI site could be cleaved, generating a DSB. ChIP–qPCR analysis was conducted to detect the presence of γH2AX, RAD51AP1, and rRNA at the targeted DSB site. Specific primers are listed in Table S1.

RNA FISH

Cells were fixed with 4% paraformaldehyde for 10 min and permeabilized by an ion buffer (0.1% Trition X-100 in PBS). These cells were then incubated with wash buffer (Bioresearch Technologies) for 10 min at 37 °C. Subsequently, the cells were incubated with probes diluted in hybridization buffer (Bioresearch Technologies) overnight at 37 °C. The probes are listed in Table S1.

Immunofluorescence staining

After fixation (4% paraformaldehyde and 0.1% Triton X-100), cells were incubated with different primary antibodies in 1% bovine serum albumin at 4 °C overnight and subsequently incubated with corresponding secondary antibody at room temperature for 1 h. Coverslips were mounted with 4′,6-diamidino-2-phenylindole Fluoromount-G (Yeason). For RNA polymerase inhibitor treatment, 1 μM pol I inhibitor (BMH-21, Selleck CAS S7718), 1 μM pol II inhibitor (α-amanitin, R&D system CAS 4025), or 50 μM pol III inhibitor (RNA polymerase III inhibitor, CAS 577784-91-9) was added to the cell culture medium for 2 h. Then, cells were exposed to 20 Gy of irradiation and recovered 12 h. To detect protein and RNA simultaneously, the slides were fixed again after immunofluorescence staining. FISH was then performed as described previously.

Western blotting

Cells were harvested in PBS and centrifuged at 12,000 rpm for 1 min. The pellet was resuspended in loading buffer (2% SDS, 100 mM DTT, 100 mM [pH 6.8] Tris–HCl, 10% glycerol, 5% 2-mercaptoethanol, and 0.0025% bromophenol blue) containing protease inhibitor cocktail and was boiled at 95 °C for 5 min. Proteins were separated on SDS-PAGE and were

transferred onto nitrocellulose membranes. The nitrocellulose membranes were incubated in blocking buffer (5% defatted milk and TBST buffer [50 mM Tris–HCl, 150 mM NaCl, and 0.1% Tween-20]) for 1 h. The primary antibody was incubated overnight at 4 °C, and the secondary antibody was incubated for 2 h at room temperature. Blot signals were captured by ChemiDoc XRS+ System using SuperSignal West Pico PLUS kit (Thermo Fisher).

Northern blotting

RNAs were extracted with TRIzol and phenol–chloroform. The concentration of RNAs was detected by NanoDrop One/OneC. RNAs were loaded to the agarose gel and separated for 4 h at 4 °C. RNAs in the agarose gel were then transferred to Amersham Hybond-N+ positively charged nylon membrane in 20× saline sodium citrate (SSC) overnight. The membranes were washed with 2× SSC and air dried at 80 °C. After UV crosslink, the membranes were hybridized with biotin-labeled probes in ULTRAhyb Ultrasensitive Hybridization Buffer at 42 °C overnight. The membranes were washed with wash buffer (0.2× SSC, 0.1% SDS) for 15 min three times at 42 °C. The blot signals were captured by ChemiDoc XRS+ System using Chemiluminescent Nucleic Acid Detection Module Kit (Thermo Scientific).

Neosynthesized protein measurement

After administration of different drugs, cells were treated with 10 μg/ml puromycin for 10 min (30). Cycloheximide-treated cells served as positive control. The cells were lysed, and neosynthesized proteins were evaluated by immunoblotting using antipuromycin antibody.

LLPS assay and FRAP

For the LLPS experiments, EGFP-RAD51AP1 proteins were incubated with different concentrations of pre-rRNA in a phase separation buffer (50 mM Tris–HCl and 10% PEG8000) for 5 min at room temperature. Each sample (20 μl) was pipetted onto a confocal dish with a coverslip. Then, the samples were imaged using Zeiss 900 confocal microscope.

The FRAP assay was performed using the bleaching module of the Zeiss 900 confocal microscope system. Briefly, the sample was bleached using 488 nm laser at 100% power. The images were captured with time-lapse module every 5 s for about 5 min. For each time point, the signal of the photobleaching site was normalized to the fluorescence intensity of the nearby site. The data of the fluorescence intensity were obtained and analyzed by ZEN 3.3.

HR efficiency assays

Tet-DR-GFP-U2OS cells were used for HR efficiency assay. The cells were transfected with pCW-HA-I-SceI-GR plasmids. Doxycycline and triamcinolone acetonide were applied to cut the I-SceI sites and generate DSBs. HR efficiency was determined by flow cytometry as reported in the previous study (31).

Statistical analysis

Statistical analyses were performed using GraphPad Prism 7 (GraphPad Software, Inc). The statistical significance was carried out by two-tailed unpaired Student's *t* test. All the data were presented as mean ± SD. The significance levels are annotated: $^{*}p < 0.05$, $^{**}p < 0.01$, and $^{***}p < 0.001$.

Data availability

All the relevant data associated with the current study can be found in the main text or supporting information. RNA-Seq data have been deposited in the Gene Expression Omnibus Datasets under the Gene Expression Omnibus accession number GSE252475.

Supporting information—This article contains supporting information.

Acknowledgments—This work was supported in part by grants from the National Natural Science Foundation of China (grant nos.: 32090034, 81874160, and 82303624), Zhejiang Provincial Natural Science Foundation of China (grant no.: 2022XHSJJ001), Hangzhou City Leading Innovation and Entrepreneurship Team (grant no.: TD2020004), "Pioneer" and "Leading Goose" R&D Program of Zhejiang (grant no.: 2024SSYS0033), Westlake University Education Foundation, and Westlake Laboratory of Life Sciences and Biomedicine. We appreciate the support of the Microscope Core Facility, General Equipment Core Facility, and Flow Cytometry Core Facility of Westlake University. We thank Dr Qilin Li for the help of data analysis.

Author contributions—L. C. conceptualization; L. C. methodology; L. C. data curation; L. C. and X. G. investigation; L. C. writing–original draft; X. G. and X. Y. writing–review & editing; X. Y. supervision.

Conflict of interest—The authors declare that they have no conflicts of interest with the contents of this article.

Abbreviations—The abbreviations used are: cDNA, complementary DNA; ChIP, chromatin immunoprecipitation; DSB, double-strand break; EGFP, enhanced GFP; FRAP, fluorescent recovery after photobleaching; GST, glutathione-S-transferase; HR, homologous recombination; IR, ionizing radiation; ITS1, internal transcribed spacer 1; LLPS, liquid–liquid phase separation; PAR-CLIP, photoactivatable ribonucleoside-enhanced crosslinking and immunoprecipitation; Pol I, RNA polymerase I; qPCR, quantitative PCR; RAD51AP1, RAD51-associated protein 1; RPA, replication protein A; SSC, saline sodium citrate.

References

1. Sung, P., and Klein, H. (2006) Mechanism of homologous recombination: mediators and helicases take on regulatory functions. *Nat. Rev. Mol. Cell Biol.* **7**, 739–750
2. Michel, B., Grompone, G., Flores, M. J., and Bidnenko, V. (2004) Multiple pathways process stalled replication forks. *Proc. Natl. Acad. Sci. U. S. A.* **101**, 12783–12788

3. McEachern, M. J., and Haber, J. E. (2006) Break-induced replication and recombinational telomere elongation in yeast. *Annu. Rev. Biochem.* **75**, 111–135
4. Lord, C. J., and Ashworth, A. (2016) BRCAness revisited. *Nat. Rev. Cancer* **16**, 110–120
5. Ranjha, L., Howard, S. M., and Cejka, P. (2018) Main steps in DNA double-strand break repair: an introduction to homologous recombination and related processes. *Chromosoma* **127**, 187–214
6. Modesti, M., Budzowska, M., Baldeyron, C., Demmers, J. A., Ghirlando, R., and Kanaar, R. (2007) RAD51AP1 is a structure-specific DNA binding protein that stimulates joint molecule formation during RAD51-mediated homologous recombination. *Mol. Cell* **28**, 468–481
7. Bzymek, M., Thayer, N. H., Oh, S. D., Kleckner, N., and Hunter, N. (2010) Double Holliday junctions are intermediates of DNA break repair. *Nature* **464**, 937–941
8. Krejci, L., Altmannova, V., Spirek, M., and Zhao, X. (2012) Homologous recombination and its regulation. *Nucleic Acids Res.* **40**, 5795–5818
9. Chen, Y., Wu, J., Zhai, L., Zhang, T., Yin, H., Gao, H., *et al.* (2024) Metabolic regulation of homologous recombination repair by MRE11 lactylation. *Cell* **187**, 294–311.e21
10. Papaspyropoulos, A., Lagopati, N., Mourkioti, I., Angelopoulou, A., Kyriazis, S., Liontos, M., *et al.* (2021) Regulatory and functional involvement of long non-coding RNAs in DNA double-strand break repair mechanisms. *Cells* **10**, 1506
11. Kovalenko, O. V., Golub, E. I., Bray-Ward, P., Ward, D. C., and Radding, C. M. (1997) A novel nucleic acid-binding protein that interacts with human rad51 recombinase. *Nucleic Acids Res.* **25**, 4946–4953
12. Wiese, C., Dray, E., Groesser, T., San Filippo, J., Shi, I., Collins, D. W., *et al.* (2007) Promotion of homologous recombination and genomic stability by RAD51AP1 via RAD51 recombinase enhancement. *Mol. Cell* **28**, 482–490
13. Liang, F., Longerich, S., Miller, A. S., Tang, C., Buzovetsky, O., Xiong, Y., *et al.* (2016) Promotion of RAD51-mediated homologous DNA pairing by the RAD51AP1-UAF1 complex. *Cell Rep.* **15**, 2118–2126
14. Parplys, A. C., Zhao, W., Sharma, N., Groesser, T., Liang, F., Maranon, D. G., *et al.* (2015) NUCKS1 is a novel RAD51AP1 paralog important for homologous recombination and genome stability. *Nucleic Acids Res.* **43**, 9817–9834
15. Dunlop, M. H., Dray, E., Zhao, W., Tsai, M. S., Wiese, C., Schild, D., *et al.* (2011) RAD51-associated protein 1 (RAD51AP1) interacts with the meiotic recombinase DMC1 through a conserved motif. *J. Biol. Chem.* **286**, 37328–37334
16. Dunlop, M. H., Dray, E., Zhao, W., San Filippo, J., Tsai, M. S., Leung, S. G., *et al.* (2012) Mechanistic insights into RAD51-associated protein 1 (RAD51AP1) action in homologous DNA repair. *J. Biol. Chem.* **287**, 12343–12347
17. Ouyang, J., Yadav, T., Zhang, J. M., Yang, H., Rheinbay, E., Guo, H., *et al.* (2021) RNA transcripts stimulate homologous recombination by forming DR-loops. *Nature* **594**, 283–288
18. Barroso-González, J., García-Expósito, L., Hoang, S. M., Lynskey, M. L., Roncaioli, J. L., Ghosh, A., *et al.* (2019) RAD51AP1 is an Essential mediator of alternative lengthening of telomeres. *Mol. Cell* **76**, 11–26.e7
19. Kaminski, N., Wondisford, A. R., Kwon, Y., Lynskey, M. L., Bhargava, R., Barroso-González, J., *et al.* (2022) RAD51AP1 regulates ALT-HDR through chromatin-directed homeostasis of TERRA. *Mol. Cell* **82**, 4001–4017.e7
20. Gai, X., Xin, D., Wu, D., Wang, X., Chen, L., Wang, Y., *et al.* (2022) Pre-ribosomal RNA reorganizes DNA damage repair factors in nucleus during meiotic prophase and DNA damage response. *Cell Res.* **32**, 254–268
21. Yang, G., Chen, Y., Wu, J., Chen, S. H., Liu, X., Singh, A. K., *et al.* (2020) Poly(ADP-ribosyl)ation mediates early phase histone eviction at DNA lesions. *Nucleic Acids Res.* **48**, 3001–3013
22. Mullineux, S. T., and Lafontaine, D. L. (2012) Mapping the cleavage sites on mammalian pre-rRNAs: where do we stand? *Biochimie* **94**, 1521–1532
23. Colis, L., Peltonen, K., Sirajuddin, P., Liu, H., Sanders, S., Ernst, G., *et al.* (2014) DNA intercalator BMH-21 inhibits RNA polymerase I independent of DNA damage response. *Oncotarget* **5**, 4361–4369
24. Michelini, F., Rossiello, F., d'Adda di Fagagna, F., and Francia, S. (2019) RNase A treatment and reconstitution with DNA damage response RNA in living cells as a tool to study the role of non-coding RNA in the formation of DNA damage response foci. *Nat. Protoc.* **14**, 1489–1508
25. Fijen, C., and Rothenberg, E. (2021) The evolving complexity of DNA damage foci: RNA, condensates and chromatin in DNA double-strand break repair. *DNA Repair (Amst)* **105**, 103170
26. Roden, C., and Gladfelter, A. S. (2021) RNA contributions to the form and function of biomolecular condensates. *Nat. Rev. Mol. Cell Biol.* **22**, 183–195
27. Feng, S., and Manley, J. L. (2022) Beyond rRNA: nucleolar transcription generates a complex network of RNAs with multiple roles in maintaining cellular homeostasis. *Genes Dev.* **36**, 876–886
28. Corley, M., Burns, M. C., and Yeo, G. W. (2020) How RNA-binding proteins interact with RNA: molecules and mechanisms. *Mol. Cell* **78**, 9–29
29. Ohle, C., Tesorero, R., Schermann, G., Dobrev, N., Sinning, I., and Fischer, T. (2016) Transient RNA–DNA hybrids are required for efficient double-strand break repair. *Cell* **167**, 1001–1013
30. Schmidt, E. K., Clavarino, G., Ceppi, M., and Pierre, P. (2009) SUnSET, A nonradioactive method to monitor protein synthesis. *Nat. Methods* **6**, 275–277
31. Chen, Q., Kassab, M. A., Dantzer, F., and Yu, X. (2018) PARP2 mediates branched poly ADP-ribosylation in response to DNA damage. *Nat. Commun.* **9**, 3233